Preprints of the 19th World Congress
The International Federation of Automatic Control
Cape Town, South Africa. August 24-29, 2014

Multirate Adaptive Compensation of Uncertain Resonances Beyond the Nyquist Frequency ⋆

Chee Khiang Pang * **Weili Yan** *,** **Chunling Du** **

* *Department of Electrical and Computer Engineering, National University of Singapore, 4 Engineering Drive 3, Singapore 117586 (e-mail: justinpang@nus.edu.sg; weiliyan@nus.edu.sg)*
** *Data Storage Institute, A*STAR, 5 Engineering Drive 1, Singapore 117608 (e-mail: Du_Chunling@dsi.a-star.edu.sg)*

Abstract: In this paper, an add-on multirate adaptive control scheme is proposed for compensation of uncertain mechanical resonant modes beyond the Nyquist frequency in mechatronic systems. A polynomial transformation technique is applied to obtain the mixed-rate model of the control system that is suitable for multirate adaptive control design. To preserve the performance of the pre-designed nominal controller, an auxiliary error is utilized in the parameter estimation process instead of tracking error. The proposed multirate adaptive control combined with a Recursive Least-Squares (RLS) algorithm and a dead-zone ensures boundedness of all the closed-loop signals and convergence of the auxiliary error. Our simulation results on the model of the Voice Coil Motor (VCM) actuator in a commercial Hard Disk Drive (HDD) demonstrate the effectiveness of our proposed compensation scheme in attenuating the mechanical resonances beyond the Nyquist frequency.

Keywords: beyond the Nyquist frequency, adaptive control, multirate control, RLS with a dead-zone

1. INTRODUCTION

In mechatronic systems, mechanical resonant modes can be easily excited by various sources such as air-flow (Yamaguchi et al. [2013]). These excited resonant modes would cause structural vibrations and degrade the control performance. Hitherto, notch filters and peak filters have been widely used to deal with structural vibrations. In practice, mass manufacturing and various operation conditions can lead to a shift in the resonant frequency, and fixed notch or peak filters may not achieve the desirable performance. To overcome this problem, adaptive notch filters or chasing peak filters that follow the resonant frequency have been developed (see Kang et al. [2005], Ohno et al. [2006], Levin et al. [2011], and Masashi [2004]). In addition, several adaptive control schemes were also proposed to compensate for uncertain resonant modes (Wu et al. [2000], Tee [2007], and Hong et al. [2010]). However, all these adaptive methods are designed for resonant modes below the Nyquist frequency.

In industries, the output sampling rate in mechatronic systems is often constrained by various factors such as manufacturing cost. Due to the aliasing effect, mechanical resonant modes beyond the Nyquist frequency can be reflected back to low frequencies, and the performance of the control system can be degraded when these low frequencies are near the servo bandwidth. In response to this problem, multirate notch filters have been proposed when the resonant mode beyond the Nyquist frequency is known a *priori* (see Weaver et al. [1995] and Cao et al. [2006]). By using the frequency response of the controlled plant, a design method was presented in (Atsumi et al. [2008]) for mechanical vibration control beyond the Nyquist frequency. However, to the best of our knowledge, no studies have been reported for compensation of uncertain resonances beyond the Nyquist frequency.

In this paper, a new multirate adaptive control scheme is proposed to compensate for uncertain resonances beyond the Nyquist frequency. A mixed-rate model catering for multirate adaptive control design is obtained through a polynomial transformation technique. To preserve properties of the nominal control, an auxiliary error instead of tracking error is used to drive the adaptive control process. A Recursive Least-Squares (RLS) algorithm with a dead-zone is presented to estimate the unknown parameters, and its convergence properties are analyzed in the presence of the bounded disturbances. Our simulation results on the model of the Voice Coil Motor (VCM) actuator in a commercial Hard Disk Drive (HDD) demonstrate the effectiveness of the proposed adaptive control.

The rest of the paper is organized as follows. Section 2 describes the problem formulation for multirate systems with uncertain resonant modes beyond the Nyquist frequency. Section 3 adopts the polynomial transformation technique to model the multirate system for adaptive control design. Section 4 presents multirate adaptive compensation scheme using a RLS algorithm with a dead-zone. Section 5 analyzes the convergence properties of the proposed

⋆ This work was supported in part by Singapore MOE AcRF Tier 1 Grant R-263-000-A44-112.

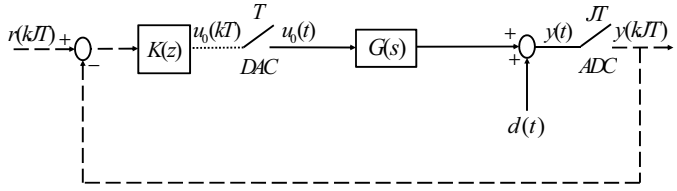

Fig. 1. Block diagram of the sampled-data control system. Solid: continuous-time signals. Dashed: discrete-time signals with sampling period JT. Dotted: discrete-time signals with sampling period T.

adaptive control. The effectiveness of the proposed control scheme is verified with simulations on a head-positioning servo control system in Section 6. Our conclusions are summarized in Section 7.

2. PROBLEM FORMULATION

Consider a sampled-data control system as shown in Fig. 1. $G(s)$ is a continuous-time Linear Time-Invariant (LTI) mechanical plant consisting of the nominal plant $G_n(s)$ and the unknown resonant mode $G_u(s)$. The pre-designed nominal controller $K(z)$ stabilizes $G_n(s)$, and $G_u(s)$ needs to be compensated. r is the nominal reference, and $d(t)$ is the lumped output disturbances. The sampling period of the input $u_0(kT)$ is T, and the sampling period of the output $y(kJT)$ is JT, where $J \in \mathbb{Z}^+ \backslash \{1\}$.

The overall plant $G(s)$ can be represented by

$$G(s) = G_n(s) + G_u(s) = \sum_{j=1}^{N_r} \frac{R_j}{s^2 + 2\zeta_j \omega_j s + \omega_j^2}, \quad (1)$$

where R_j, ζ_j, and ω_j are the residue, damping ratio, and natural frequency of N_r resonant modes. It is assumed that $G(s) \in RH_\infty$.

From Fig. 1, the Nyquist frequency of the output sampling rate is $\frac{1}{2JT}$. We consider that $G(s)$ contains unknown resonant modes with natural frequencies beyond $\frac{1}{2JT}$ but below $\frac{1}{2T}$. The objective of this paper is to design an add-on multirate adaptive discrete-time controller with the faster sampling period T to compensate for the unknown resonances beyond the Nyquist frequency, while maintaining the performance of the nominal controller.

The block diagram of the proposed multirate adaptive compensation scheme is illustrated in Fig. 2. $G_n(z)$ and $G_u(z)$ are the discrete transfer functions of $G_n(s)$ and $G_u(s)$, respectively, using the zero-order hold equivalence method with period T. S_{JT} is a down-sampler with period JT. $u_1(kT)$ is an add-on control input, and the disturbance $d(kT)$ is bounded, i.e., $|d(kT)| \le \bar{d}$, where $|\cdot|$ denotes the absolute value operator. $y^*(kT)$ is the ideal output if $G_u(z) = 0$ and $d(kT) = 0$. To compensate for the resonant mode $G_u(z)$ and maintain the performance of the nominal closed-loop system, $u_1(kT)$ is designed to make an auxiliary error $e(kT) = y(kT) - y^*(kT)$ as small as possible in the presence of the disturbance.

Let q^{-1} denote the backward shift operator with sampling period T. The discrete transfer function $G(z)$ can be expressed by $G(q^{-1})$ with the operator q^{-1}. From Fig. 2,

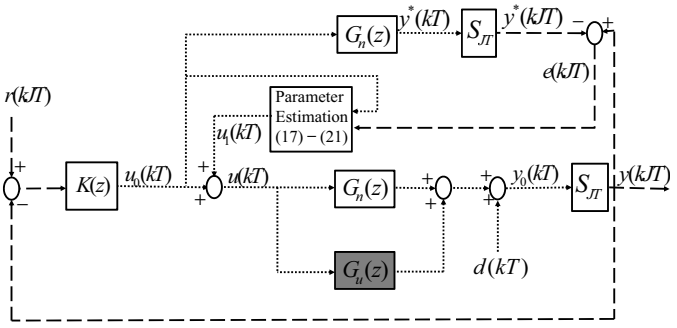

Fig. 2. Multirate adaptive discrete-time control system. Dashed: discrete-time signals with sampling period JT. Dotted: discrete-time signals with sampling period T.

$$y_0(kT) = G(q^{-1})u(kT) + d(kT), \quad (2)$$

where

$$G(q^{-1}) = G_n(q^{-1}) + G_u(q^{-1}) = \frac{B_n(q^{-1})}{A_n(q^{-1})} + \frac{B_u(q^{-1})}{A_u(q^{-1})} = \frac{B_0(q^{-1})}{A_0(q^{-1})}. \quad (3)$$

Since $y(kJT)$ is generated from the fictitious output $y_0(kT)$ through the down-sampler S_{JT}, we have

$$y(kJT) = y_0(kJT), \ k = 0, 1, 2, \cdots. \quad (4)$$

Replacing k with kJ in (2) and using (4),

$$y(kJ) = G(q^{-1})u(kJ) + d(kJ), \quad (5)$$

where $T = 1$ is used for notational simplicity.

Furthermore, the auxiliary error can be expressed as

$$\begin{aligned} e(kJ) &= y(kJ) - y^*(kJ) \\ &= G_u(q^{-1})u_0(kJ) + G(q^{-1})u_1(kJ) + d(kJ) \\ &= \frac{A_n(q^{-1})B_u(q^{-1})}{A_n(q^{-1})A_u(q^{-1})}u_0(kJ) \\ &\quad + \frac{A_n(q^{-1})B_u(q^{-1}) + A_u(q^{-1})B_n(q^{-1})}{A_n(q^{-1})A_u(q^{-1})}u_1(kJ) \\ &\quad + d(kJ). \end{aligned} \quad (6)$$

The system dynamics in (6) can be written as

$$\begin{aligned} A_0(q^{-1})[e(kJ) - d(kJ)] &= B_0(q^{-1})u_1(kJ) \\ &\quad + C_0(q^{-1})u_0(kJ), \end{aligned} \quad (7)$$

where $A_0(q^{-1})$ is Hurwitz, and

$$\begin{aligned} A_0(q^{-1}) &= 1 + a_1 q^{-1} + a_2 q^{-2} + \cdots + a_n q^{-n}, \\ B_0(q^{-1}) &= b_1 q^{-1} + b_2 q^{-2} + \cdots + b_n q^{-n}, \\ C_0(q^{-1}) &= c_1 q^{-1} + c_2 q^{-2} + \cdots + c_n q^{-n}. \end{aligned} \quad (8)$$

Based on (7), it is easy to design an indirect adaptive controller when $e(k)$ is available at each sampling point with period T. However, $\{ e(kJ + i), i = 1, 2, \cdots, J - 1 \}$ is unavailable due to the slow output sampling rate. In the

following section, a polynomial transformation technique in (Lu et al. [1989]) is used to transform the model of (7) into a mixed-rate model that is suitable for multirate adaptive control design.

3. MODELING BASED ON POLYNOMIAL TRANSFORMATION TECHNIQUE

Rewrite $A_0(q^{-1})$ as

$$\begin{aligned} A_0(q^{-1}) &= 1 + a_1 q^{-1} + a_2 q^{-2} + \cdots + a_n q^{-n} \\ &= \prod_{l=1}^{n} [1 - (\lambda_l q)^{-1}], \end{aligned} \tag{9}$$

where λ_l is a root of $A_0(q^{-1})$.

Multiplying both sides of (7) with

$$\prod_{l=1}^{n} [1 + (\lambda_l q)^{-1} + (\lambda_l q)^{-2} + \cdots + (\lambda_l q)^{1-J}], \tag{10}$$

the following mixed-rate model

$$A(q^{-J})e(kJ) = B(q^{-1})u_1(kJ) + C(q^{-1})u_0(kJ) + D(kJ) \tag{11}$$

can be obtained, where $D(kJ) = A(q^{-J})d(kJ)$, and

$$\begin{aligned} A(q^{-J}) &= 1 + \alpha_J q^{-J} + \alpha_{2J} q^{-2J} + \cdots + \alpha_{nJ} q^{-nJ} \\ B(q^{-1}) &= \beta_1 q^{-1} + \beta_2 q^{-2} + \cdots + \beta_{nJ} q^{-nJ} \\ C(q^{-1}) &= \gamma_1 q^{-1} + \gamma_2 q^{-2} + \cdots + \gamma_{nJ} q^{-nJ}. \end{aligned} \tag{12}$$

Rewrite the model in (11) as

$$e(kJ) = \phi_0^T(kJ-1)\theta_0 + u_1(kJ-1)\beta_1 + D(kJ), \tag{13}$$

where

$$\begin{aligned} \phi_0(kJ-1) = [&-e(kJ-J), \cdots, -e(kJ-nJ), \\ &u_1(kJ-2), \cdots, u_1(kJ-nJ), \\ &u_0(kJ-1), \cdots, u_0(kJ-nJ)]^T, \end{aligned} \tag{14}$$

and

$$\theta_0 = [\alpha_J, \alpha_{2J}, \cdots, \alpha_{nJ}, \beta_2, \beta_3, \cdots, \beta_{nJ}, \gamma_1, \gamma_2, \cdots, \gamma_{nJ}]^T. \tag{15}$$

Define $\phi(kJ-1) = [\phi_0^T(kJ-1), u_1(kJ-1)]^T \in \mathbb{R}^{n+2nJ}$ and $\theta = [\theta_0^T, \beta_1]^T \in \mathbb{R}^{n+2nJ}$. Rewrite (13) as

$$e(kJ) = \phi^T(kJ-1)\theta + D(kJ). \tag{16}$$

Based on the model in (13), an indirect multirate adaptive control scheme is presented in the following section to make $e(k)$ as small as possible, while ensuring boundedness of all the closed-loop signals.

4. MULTIRATE ADAPTIVE CONTROL DESIGN

To make the control problem solvable, two assumptions are introduced as follows.

Assumption 1. The sign of β_1 is known. Without loss of generality, we assume $\beta_1 \geq \underline{\beta} > 0$, i.e., the relative degree of the system is one.

Assumption 2. The disturbance $D(k)$ is bounded, i.e., $|D(k)| \leq \bar{D}$.

Let $\hat{\theta}_0(kJ)$ and $\hat{\beta}_1(kJ)$ denote the estimates for θ_0 and β_1 at the time instant kJ, respectively. The proposed adaptive control law at the time instant $(kJ-1)$ is

$$u_1(kJ-1) = -\frac{\phi_0^T(kJ-1)\hat{\theta}_0(kJ-J)}{\hat{\beta}_1(kJ-J)}, \tag{17}$$

where all the elements in $\phi_0^T(kJ-1)$ at the current time are all available.

For the time instants $\{kJ+i-1, i = 1, 2, \cdots, J-1\}$, the adaptive control law is

$$u_1(kJ+i-1) = -\frac{\hat{\phi}_0^T(kJ+i-1)\hat{\theta}_0(kJ-J)}{\hat{\beta}_1(kJ-J)}, \tag{18}$$

where

$$\begin{aligned} \hat{\phi}_0(kJ+i-1) = [&0, \cdots, 0, \\ &u_1(kJ+i-2), \cdots, u_1(kJ+i-nJ), \\ &u_0(kJ+i-1), \cdots, u_0(kJ+i-nJ)]^T. \end{aligned} \tag{19}$$

It is worth noting that the unavailable inter-sample errors $\{e(kJ+i), i = 1, 2, \cdots, J-1\}$ are replaced by zeros in $\hat{\phi}_0^T(kJ+i-1)$. Such a choice is to ensure $e(kJ+i)$ converges to a small neighborhood of zero.

The RLS-based parameter update law with a dead-zone is

$$\begin{aligned} \hat{\theta}(kJ) = \wp\Bigg\{ &\hat{\theta}(kJ-J) + \\ &\frac{\mu(kJ)\nu(kJ)P(kJ-J)\phi(kJ-1)e(kJ)}{1+\mu(kJ)\nu(kJ)\phi^T(kJ-1)P(kJ-J)\phi(kJ-1)} \Bigg\}, \end{aligned} \tag{20}$$

$$\begin{aligned} P(kJ) = &P(kJ-J) - \\ &\frac{\mu(kJ)\nu(kJ)P(kJ-J)\phi(kJ-1)\phi^T(kJ-1)P(kJ-J)}{1+\mu(kJ)\nu(kJ)\phi^T(kJ-1)P(kJ-J)\phi(kJ-1)}, \end{aligned} \tag{21}$$

where $\mu(kJ)$ and $\nu(kJ)$ are given by

$$\mu(kJ) = \frac{|e(kJ)|\bar{D}^{-1} - 1}{1 + \phi^T(kJ-1)P(kJ-J)\phi(kJ-1)}, \tag{22}$$

$$\nu(kJ) = \begin{cases} 0 \ , |e(kJ)| < \bar{D}, \\ 1 \ , |e(kJ)| \geq \bar{D}. \end{cases} \tag{23}$$

Let $\mathbf{x} = [\mathbf{x}_0^T, x_1]^T$ denote the vector $\hat{\theta}(kJ-J) + \frac{\mu(kJ)\nu(kJ)P(kJ-J)\phi(kJ-1)e(kJ)}{1+\mu(kJ)\nu(kJ)\phi^T(kJ-1)P(kJ-J)\phi(kJ-1)}$. The operator $\wp\{\mathbf{x}\}$ is

$$\wp\{\mathbf{x}\} = \begin{cases} [\mathbf{x}_0^T, x_1]^T \ , x_1 > \underline{\beta}, \\ [\mathbf{x}_0^T, \underline{\beta}]^T \ , x_1 \leq \underline{\beta}. \end{cases} \tag{24}$$

It can be noted that the modification in (24) can avoid the singularity problem of the control laws in (17) and (18).

5. CONVERGENCE ANALYSIS

In this section, the convergence properties of the proposed adaptive control are summarized in the following theorem.

Theorem 1. For the system in (13), under Assumptions 1-2, the control laws in (17) and (18), and the parameter update laws in (20)–(21) guarantee boundedness of all the closed-loop signals. The following properties are ensured:

(i) For $\{e(kJ), k = 0, 1, \cdots\}$,

$$\lim_{k\to\infty} \sup |e(kJ)| \le \bar{D}. \tag{25}$$

(ii) For the tracking error $\varepsilon(kJ) = r(kJ) - y(kJ)$,

$$\lim_{k\to\infty} \sup |\varepsilon(kJ)| \le \bar{S}(\bar{r} + \bar{D}), \tag{26}$$

where $|\frac{1}{1+K(e^{j\omega T})G_n(e^{j\omega T})}| \le \bar{S}$ and $|r(kJ)| \le \bar{r}$.

Proof. (i) From (17),

$$\begin{aligned} 0 &= \phi_0^T(kJ-1)\hat{\theta}_0(kJ-J) + u_1(kJ-1)\hat{\beta}_1(kJ-J) \\ &= \phi^T(kJ-1)\hat{\theta}(kJ-J). \end{aligned} \tag{27}$$

By subtracting (16) from (27), we obtain

$$e(kJ) = -\phi^T(kJ-1)\tilde{\theta}(kJ-J) + D(kJ), \tag{28}$$

where $\tilde{\theta}(kJ) = \hat{\theta}(kJ) - \theta$.

According to the matrix inversion lemma, (21) implies

$$\begin{aligned} P^{-1}(kJ) = P^{-1}(kJ-J) \\ +\mu(kJ)\nu(kJ)\phi(kJ-1)\phi^T(kJ-1). \end{aligned} \tag{29}$$

Using $\beta_1 \ge \underline{\beta}$ in Assumption 1, it can be known that

$$(\wp\{\mathbf{x}\} - \theta)^T(\wp\{\mathbf{x}\} - \theta) \le (\mathbf{x} - \theta)^T(\mathbf{x} - \theta). \tag{30}$$

Furthermore, since $P^{-1}(kJ)$ is symmetric positive definite,

$$\begin{aligned} &(\wp\{\mathbf{x}\} - \theta)^T P^{-1}(kJ)(\wp\{\mathbf{x}\} - \theta) \\ &\le (\mathbf{x} - \theta)^T P^{-1}(kJ)(\mathbf{x} - \theta). \end{aligned} \tag{31}$$

Define $V(kJ) = \tilde{\theta}^T(kJ)P^{-1}(kJ)\tilde{\theta}(kJ)$. Using (20) and (28)–(31) yields

$$\begin{aligned} &V(kJ) - V(kJ-J) \\ &\le \mu(kJ)\nu(kJ)D^2(kJ) \\ &\quad - \frac{\mu(kJ)\nu(kJ)e^2(kJ)}{1+\mu(kJ)\nu(kJ)\phi^T(kJ-1)P(kJ-J)\phi(kJ-1)}. \end{aligned} \tag{32}$$

Based on (23), the following two cases are discussed.

Case 1: if $|e(kJ)| < \bar{D}$, $\nu(kJ) = 0$, hence

$$V(kJ) - V(kJ-J) \le 0. \tag{33}$$

Case 2: if $|e(kJ)| \ge \bar{D}$, $\nu(kJ) = 1$, $\mu(kJ) \ge 0$, hence

$$\begin{aligned} &D^2(kJ)[1 + \mu(kJ)\phi^T(kJ-1)P(kJ-J)\phi(kJ-1)] \\ &\le D^2(kJ)\frac{|e(kJ)|}{\bar{D}} \le \bar{D}|e(kJ)|. \end{aligned} \tag{34}$$

Using (32), (34) leads to

$$\begin{aligned} &V(kJ) - V(kJ-J) \\ &\le \frac{\mu(kJ)(\bar{D}|e(kJ)| - e^2(kJ))}{1+\mu(kJ)\phi^T(kJ-1)P(kJ-J)\phi(kJ-1)} \\ &= -\frac{(|e(kJ)| - \bar{D})^2}{\frac{\bar{D}}{|e(kJ)|} + \phi^T(kJ-1)P(kJ-J)\phi(kJ-1)} \\ &\le -\frac{(|e(kJ)| - \bar{D})^2}{1+\phi^T(kJ-1)P(kJ-J)\phi(kJ-1)}. \end{aligned} \tag{35}$$

Summarizing these two cases, it can be concluded that

$$\begin{aligned} &V(kJ) - V(kJ-J) \\ &\le -\frac{\nu(kJ)(|e(kJ)| - \bar{D})^2}{1+\phi^T(kJ-1)P(kJ-J)\phi(kJ-1)} \le 0, \end{aligned} \tag{36}$$

which indicates $V(kJ)$ is non-increasing with respect to k.

It is straightforward to prove that

$$\|\tilde{\theta}(kJ)\|^2 \le \frac{\lambda_{max}(P^{-1}(0))}{\lambda_{min}(P^{-1}(0))}\|\tilde{\theta}(0)\|^2, \tag{37}$$

which indicates boundedness of all the closed-loop signals.

In view of (36), we have

$$\lim_{k\to\infty} \frac{\nu(kJ)(|e(kJ)| - \bar{D})^2}{1+\phi^T(kJ-1)P(kJ-J)\phi(kJ-1)} = 0. \tag{38}$$

Using the key technical lemma in (Goodwin et al. [1980]), it is easy to obtain

$$\lim_{k\to\infty} \nu(kJ)(|e(kJ)| - \bar{D}) = 0. \tag{39}$$

Furthermore, using (23) ensures that

$$\lim_{k\to\infty} \sup |e(kJ)| \le \bar{D}, \tag{40}$$

which gives the property in (i).

(ii) The tracking error $\varepsilon(kJ)$ can be rewritten as

$$\varepsilon(kJ) = \frac{1}{1+K(q^{-1})G_n(q^{-1})}[r(kJ) - e(kJ)] \tag{41}$$

which straightforwardly ensures (ii).

The property of the inter-sample auxiliary errors is given in the following lemma.

Lemma 1. For the system in (13), if the conditions of Theorem 1 hold and the system is persistently excited, then the inter-sample errors $\{e(kJ+i), i = 1, 2, \cdots, J-1\}$ are bounded, i.e.,

$$\lim_{k\to\infty} \sup |e(kJ+i)| \le \bar{d}. \tag{42}$$

Proof. If the system is persistently excited, we can easily obtain from Theorem 1 that

$$\lim_{k\to\infty} \tilde{\theta}(kJ-J) = 0. \tag{43}$$

From (18),

$$\begin{aligned} 0 &= \hat{\phi}_0^T(kJ+i-1)\hat{\theta}_0(kJ-J) + u_1(kJ-1)\hat{\beta}_1(kJ-J) \\ &= \hat{\phi}^T(kJ+i-1)\hat{\theta}(kJ-J), \end{aligned} \tag{44}$$

where $\hat{\phi}(kJ+i-1) = [\hat{\phi}_0^T(kJ+i-1), u_1(kJ-1)]^T$.

Combining (11) and (44), $e(kJ+i)$ can be expressed as

$$\begin{aligned} e(kJ+i) = &-\sum_{l=1}^{n} \alpha_{lJ} e(kJ+i-lJ) + D(kJ+i) \\ &-\hat{\phi}^T(kJ+i-1)\tilde{\theta}(kJ-J), \end{aligned} \tag{45}$$

which leads to

$$e(kJ+i) = -\frac{\hat{\phi}^T(kJ+i-1)\tilde{\theta}(kJ-J)}{A(q^{-J})} + d(kJ+i). \tag{46}$$

Furthermore, $\hat{\phi}^T(kJ+i-1)$ is bounded because all the closed-loop signals are bounded. Since $A(q^{-J})$ is strictly stable and $|d(k)| \le \bar{d}$, (43) implies that

$$\lim_{k\to\infty} \sup |e(kJ+i)| \le \bar{d}, \tag{47}$$

which the property in Lemma 1 is ensured.

6. SIMULATION EXAMPLE

The model of the VCM actuator in a commercial HDD is considered for our simulations. The model of the known nominal plant $G_n(s)$ is given by

$$\begin{aligned} G_n(s) = &\frac{5.6\times 10^7}{s^2+414.7s+1.421\times 10^5} \\ &+\frac{-2.1\times 10^8}{s^2+5121s+2.622\times 10^9}. \end{aligned} \tag{48}$$

For the purpose of our simulations, the model of the unknown resonant mode $G_u(s)$ is assumed as

$$G_u(s) = \frac{3.85\times 10^8}{s^2+3072s+1.049\times 10^{10}}, \tag{49}$$

where the natural frequency of $G_u(s)$ is 16.3 kHz. The frequency response of $G(s)$ is plotted in Fig. 3. Without loss of generality, the order $n = 6$ is known a *priori*.

Our proposed control scheme is carried out during track-following mode, i.e., $r(kJ) = 0$. In our simulations, $T = 2.5\times 10^{-5}$ sec and $J = 2$ are chosen. As such, the input and output sampling rates are 40 kHz and 20 kHz, respectively. The nominal controller $K(z)$ is designed as a lead-lag filter, which is given by

$$K(z) = \frac{z^2-1.96z+0.9607}{z^2-1.685z+0.685}. \tag{50}$$

The VCM actuator is subject to the disturbance model in the HDD Benchmark Problem (Yamaguchi et al. [2011]), which is represented by $d(k)$ as shown in Fig. 2. The disturbances satisfy Assumption 2 and include flutter disturbance, Repeatable Run-Out (RRO), and measurement

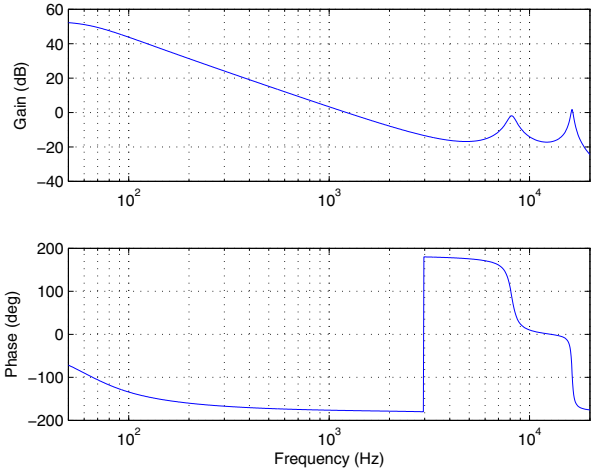

Fig. 3. Frequency response of the VCM actuator $G(s)$.

noise. It should be noted that the RRO is removed in our simulations. In practice, the RRO can be canceled by averaging the Position Error Signal (PES) and injecting sinusoidal signals with the inverse of the sensitivity function with respect to the output sampling rate. It is worth noting that no external persistently exciting signals are used in our simulations.

The proposed adaptive control scheme from (17) to (21) is applied to compensate for $G_u(s)$. The initial values are $\hat{\theta}_0(0) = \mathbf{0}_{29\times 1}$, $P(0) = 10^{12}\mathbf{I}_{30\times 30}$, $\hat{\beta}(0) = 0.03$, $\underline{\beta} = 0.01$, and $\bar{D} = 5\times 10^{-10}$. Define $\varepsilon(kJ) = -y(kJ)$ as the PES. Fig. 4 shows the convergence history of the components $\{\hat{\alpha}_J, \hat{\alpha}_{2J}, \cdots, \hat{\alpha}_{nJ}\}$ in $\hat{\theta}(kJ)$. Fig. 5 shows the transient performance of the PES before and after the adaptive compensation. It can be clearly seen that the PES decreases using the proposed adaptive compensation, as compared to that using the nominal control only.

When $k = 80000$, we stop updating the parameter estimates. By calculating the power spectrum of $\varepsilon(kJ)$, the performance of the proposed scheme is investigated. The power spectra of $\varepsilon(kJ)$ before and after the compensation are shown in Fig. 6. As can be seen, when only the nominal control is used, much PES is trapped around the frequency 3.7 kHz corresponding to the VCM actuator's mode at the resonant frequency of 16.3 kHz (due to the aliasing effect, the resonance at 16.3 kHz is reflected back on 3.7 kHz in the spectrum with the output sampling rate 20 kHz). However, using the proposed scheme, the amplitude of PES around this frequency is significantly attenuated, while the amplitudes of PES at other frequencies are almost the same as that using the nominal control only.

7. CONCLUSION

This paper has designed a multirate adaptive discrete-time controller for compensation of uncertain mechanical resonant modes beyond the Nyquist frequency. As compared to the conventional adaptive control, the proposed method utilizes an auxiliary error instead of tracking error to drive the parameter estimation process. The multirate adaptive control law has been designed using the polynomial transformation technique and the RLS algorithm

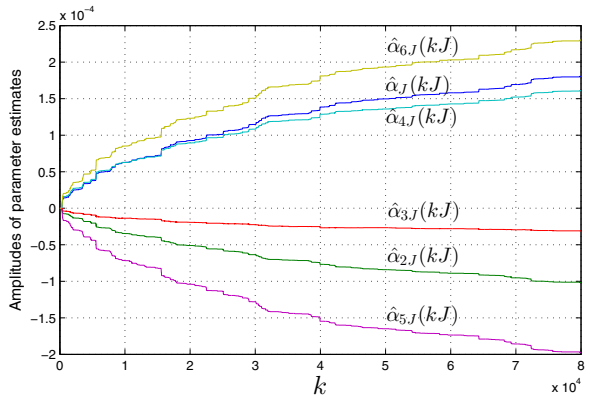

Fig. 4. Convergence history of the parameter estimates.

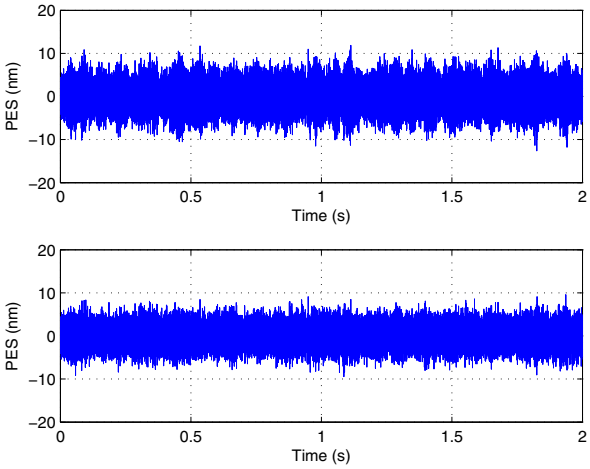

Fig. 5. Trajectory of PES during adaptation. Top: before adaptive compensation. Bottom: after adaptive compensation.

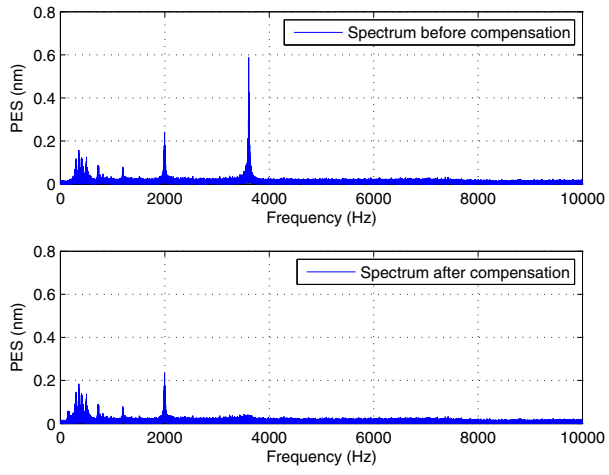

Fig. 6. Spectrum of PES before and after adaptive compensation.

with a dead-zone. The proposed control scheme can guarantee that the auxiliary error converges to a small neighborhood of zero, while all the signals in the closed-loop system remain bounded. The simulation study conducted on the model of the VCM actuator in a commercial HDD has illustrated that the proposed adaptive compensator can effectively suppress uncertain resonances beyond the Nyquist frequency, while maintaining the nominal control performance.

REFERENCES

T. Yamaguchi, M. Hirata M, and C. K. Pang (eds.). Advances in High-Performance Motion Control of Mechatronic System. CRC Press, Taylor and Francis Group, Boca Raton, FL, USA, 2013.

C. Kang and C. Kim. An adaptive notch filter for suppressing mechanical resonance in high track density disk drives. *Microsystem Technologies*, 11: 638–652, 2005.

K. Ohno and T. Hara. Adaptive resonant mode compensation for hard disk drives. *IEEE Transactions on Industrial Electronics*, 53(2): 624–630, 2006.

D. Wu, G. Guo, and T.C. Chong. Adaptive compensation of microactuator resonance mode in hard disk drives. *IEEE Transactions on Magnetics*, 36(5): 2247–2250, 2000.

J. Levin, N. Perez, and P. Ioannou. Adaptive notch filter using real-time parameter estimation. *IEEE Transactions on Control Systems Technology*, 19(3): 673–681, 2011.

K.P. Tee, S.S. Ge. and E.H. Tay. Adaptive resonance compensation for hard disk drive servo systems. In *Proceedings of the* 46^{th} *IEEE Conference on Decision and Control*, pages 3567–3572, 2007.

F. Hong, C. Du, K.P. Tee, and S.S. Ge. Adaptive disturbance rejection in the presence of uncertain resonance mode in hard disk drives. *Transactions of the Institute of Measurement and Control*, 3(2): 99–199, 2010.

P.A. Weaver and R.M. Enrlich. The use of multirate notch filters in embedded-servo disk drives. In *Proceedings of the American Control Conference*, pages 4156–4160, 1995.

W. Cao, D. Ming, and K. Ooi. Servo systems using multi-rate notch filters to attenuate resonances beyond Nyquist rate. In *Proceedings of the* 9^{th} *International Conference on Control, Automation, Robotics and Vision*, pages 1–6, 2006.

K. Masashi. Frequency chasing peak filter. *Papers of Technical Meeting on Industrial Instrumentation and Control, IEE Japan (in Japanese)*, 4: 19–23, 2004.

T. Atsumi, A. Okuyama, and S. Nakagawa. Vibration control beyond the Nyquist frequency in hard disk drives. *IEEE Transactions on Industrial Electronics*, 55(10): 3751–3757, 2008.

W. Lu and D. Fisher. Least-squares output estimation with multirate sampling. *IEEE Transactions on Automatic Control*, 34(6): 669–672, 1989.

G.C. Goodwin, P.J. Ramadge, and P.E. Caines. Discrete-time multivariable adaptive control. *IEEE Transactions on Automatic Control*, 25(3): 449–456, 1980.

T. Yamaguchi, M. Hirata M, and C. K. Pang (eds.). High-Speed Precision Motion Control, Chapter 7. CRC Press, Taylor and Francis Group, Boca Raton, FL, USA, 2011.